RSC Advances

PAPER

View Article Online
View Journal | View Issue

Cite this: *RSC Adv.*, 2020, **10**, 15541

A simple and cost-effective approach to fabricate tunable length polymeric microneedle patches for controllable transdermal drug delivery†

Yongli Chen,[ab] Yiwen Xian,[c] Andrew J. Carrier,[d] Brian Youden,[de] Mark Servos,[e] Shufen Cui,[c] Tiangang Luan,[b] Sujing Lin*[a] and Xu Zhang*[d]

Received 12th February 2020
Accepted 13th April 2020

DOI: 10.1039/d0ra01382j

rsc.li/rsc-advances

Polymeric microneedles (MNs) are attractive transdermal drug delivery systems because of their efficient drug delivery and minimal invasiveness. Master template fabrication is the most time-consuming and costly step in producing polymeric MNs using a micromoulding approach. Herein, this issue is addressed by modifying tattoo needle cartridges by adjusting the volume of a PDMS spacer, thus streamlining polymeric MN fabrication and significantly reducing its manufacturing cost. Using the fabricated master template, dissolvable polymeric MN systems containing poly(vinyl pyrrolidone) (PVP) and poly(vinyl alcohol) (PVA) were developed. This MN system exhibits several advantages, including controllable MN length, uniform distribution of each needle, and controllable drug release profiles. Overall, polymeric MN fabrication using this method is inexpensive, simple, and yields controllable and effective transdermal drug delivery.

1. Introduction

Microneedles (MNs) are a new set of transdermal drug delivery systems (TDDSs) consisting of a microstructure of cone-shaped bodies (<1 mm in length) on a flat base.[1,2] MNs enhance the transport of vaccines,[3] proteins,[4,5] nucleic acids,[6] small molecular drugs,[7–10] and nanomedicines[11–13] across the skin barrier with minimal pain and invasiveness. Therefore, they are considered a novel and effective approach to transdermal drug delivery.[14,15] MNs have been fabricated from various materials,[16,17] including silicon, silicon dioxide, metals, polymers, and SU-8 photoresist. Among these, polymeric MNs have attracted great attention because of the advantages of biocompatibility, biodegradability, flexible drug loading capability, convenient administration, low cost, and easy fabrication.[18] Meanwhile, polymeric MNs are a suitable vehicle for thermally unstable drugs, such as proteinaceous vaccines and enzymes, maintaining their bioactivity while reducing associated cold storage costs during storage and transportation.[19] In addition, various functional nanomaterials, such as photothermal nanomaterials, have been incorporated into MNs, to endow new functions or properties to the MNs,[20,21] *e.g.*, to achieve controlled cargo release or self-sterilization.[22,23]

Several polymeric MN patch fabrication methods have been developed,[24] including micromoulding,[25] droplet-born air blowing (DAB),[26] photolithography,[27,28] 3D printing,[29,30] drawing lithography,[31] and electro-drawing.[32] Among these technologies, micromoulding is the most widely used because of its simple fabrication procedure, scale up feasibility, high reproducibility, and cost-effectiveness.[18] The micromoulding fabrication procedure consists of five steps: preparing the master MN template; fabricating the female MN mould; bubble-free filling of the female mould with the polymer solution; polymer solidification; and removing the polymeric MN patch from the female mould. The preparation of a high-precision master template is the first and most important step for polymeric MN fabrication. However, the current techniques for master template fabrication, such as laser etching, deep-reactive ion etching, and anisotropic wet etching, are challenging because they require skilled personnel and expensive facilities, such as photoetching equipment and a clean room.[25,33] It often costs thousands of US dollars to fabricate one MN master template. In addition, the master templates fabricated using traditional approaches are not tunable. A new template is required to even adjust the MN length, which makes the MN optimization a tedious and costly process.[8,34,35]

To address the above-mentioned issues, we developed a simple and cost-effective method to fabricate tunable length

[a]*Postdoctoral Innovation Practice Base, Shenzhen Polytechnic, Shenzhen, 518055, China*

[b]*State Key Laboratory Biocontrol, School of Marine Sciences, Sun Yat-sen University, Guangzhou 510275, China*

[c]*Department of Biological Applied Engineering, Shenzhen Key Laboratory of Fermentation Purification and Analysis, Shenzhen Polytechnic, Shenzhen, 518055, China. E-mail: linsujing@szpt.edu.cn*

[d]*Department of Chemistry, Cape Breton University, 1250 Grand Lake Road Sydney, Nova Scotia, B1P 6L2, Canada. E-mail: xu_zhang@cbu.ca*

[e]*Department of Biology, University of Waterloo, Waterloo, Ontario, N2L 3G1, Canada*

† Electronic supplementary information (ESI) available. See DOI: 10.1039/d0ra01382j

polymeric MN patches. Unlike other fabrication methods, the MN template was fabricated by modifying commercial stainless-steel MN arrays as the master template, which are cost efficient and commonly used as a tattoo needle cartridge. Poly(-vinylpyrrolidone) (PVP) and poly(vinyl alcohol) (PVA) were used to fabricate the polymeric MN patches. By adjusting the PDMS spacer volume on the template, the polymeric MN length can be tuned. Using this fabrication method, the polymeric MN patches were uniformly distributed with high precision and reproducibility. Importantly, using the fabricated MNs, controlled drug release was achieved by changing the PVP/PVA composition or including photothermal CuS nanoparticles for near infrared irradiation (NIR)-activatable drug release. Altogether, this new approach makes polymeric MN fabrication easy, quick, and cost-effective, and it could be widely used for MN research and applications.

2. Materials and methods

2.1 Materials

Poly(vinylpyrrolidone) (PVP 30 K, MW = 30 000 daltons, molecular biology grade) was obtained from Sangon Biotech (Shanghai, China). Copper(II) chloride dihydrate ($CuCl_2 \cdot 2H_2O$, purity 99.99%) was obtained from Macklin (Shanghai, China). Poly(vinyl alcohol) (PVA, MW = 89 000–98 000 daltons, purity 99.5%), sodium sulfide ($Na_2S \cdot 9H_2O$, purity ≥ 98.0%), and fluorescein isothiocyanate (FITC) were purchased from Sigma-Aldrich (St. Louis, MO, USA). Trisodium citrate ($C_6H_5O_7Na_3$, purity 99%) was purchased from J&K (Shanghai, China). A polydimethylsiloxane kit (prepolymer and crosslinker, Sylgard 184) was purchased from Dow Corning (Midland, MI, USA). The metal microneedle cartridges were purchased from Chuanqimei Equipment Co., Ltd. (Shenzhen, China).

2.2 Synthesis and characterization of CuS nanoparticles (NPs)

The CuS NPs were synthesized by a previously reported method.[36,37] First, 55 mg of copper(II) chloride dihydrate (final concentration, 1.6 mM) and 50 mg of sodium citrate (final concentration, 0.68 mM) were dissolved in 50 mL of water. The mixture was stirred for 30 min at ambient temperature. Second, 50 μL of aqueous sodium sulfide (3.125 M) was added to the mixture and stirred for 10 min at ambient temperature to generate a dark-brown solution. Third, the reaction was heated in a 95 °C oil bath for 15 min, and the solution turned dark green. Finally, the solution was transferred to an ice water bath. After cooling, the CuS NP solution was centrifuged and then resuspended in PBS for use. The size and morphology of CuS NPs were characterized by TEM using a Hitachi HT7700 microscope operated with an accelerating voltage of 80 kVb following the established procedure. The hydrodynamic size of the CuS NPs were measured with a Malvern Zetasizer Nano ZS90 (Malvern Instruments, Worcestershire, UK). The UV-Vis spectra of the CuS NPs was recorded using a M1000 Pro plate reader (TECAN, USA).

2.3 Fabrication of the microneedle (MN) mould

As shown in Fig. 1a, a stainless-steel tattoo cartridge with MNs arranged in five rows in a configuration of 5, 10, 12, 10, and 5 MNs was used as the master template for the female MN mould fabrication. The female MN mould was fabricated by the following process: (1) preparation of the tunable master template using a PDMS spacer: the master template was surrounded by an adhesive tape to form a container to which a mixture of PDMS pre-polymer and cross-linker (10 : 1, w/w) with total volume of 100 μL was added and cured at 80 °C for 2 h. The volume of the PDMS spacer determined the length of the final MNs; (2) formation of a non-stick layer: 20 μL of 1% (w/v) PVA solution was added onto the spacer and cured at 80 °C for 10 min to form a non-stick layer to facilitate removal of the female mould; (3) preparation of PDMS-based female templates: a microwell with diameter of 1.1 cm was filled with a mixture of PDMS pre-polymer and cross-linker (10 : 1, w/w) and the air bubbles were removed by maintaining a partial vacuum. Then the prepared master template was placed slowly onto the microwell, which was then transferred into an 80 °C oven for 2 h to set; (4) demoulding: the template and PDMS were separated from the microwell plate, and then the female PDMS mould was carefully removed from the master template vertically.

2.4 Fabrication and characterization of the PVA/PVP MNs

PVP and PVA were selected for MN patch fabrication. PVA and PVP in ratios of 3 : 10, 5 : 10, and 6 : 10 with 500 mg mL^{-1} PVP solution were prepared in deionized water, respectively. Then, the solutions were centrifuged at 10 000 rpm for 5 min to remove air bubbles. After surface modification of the PDMS

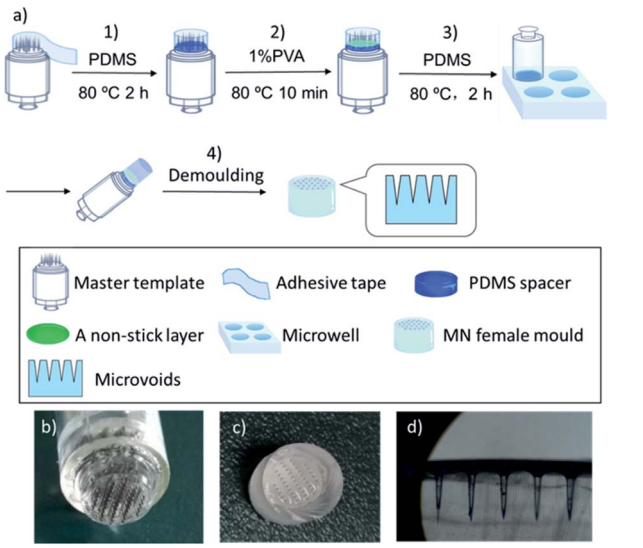

Fig. 1 (a) Microneedle female mould fabrication procedure, containing four steps: (1) preparation of the tunable master template using a PDMS spacer, (2) formation of a non-stick layer, (3) preparation of female templates, and (4) demoulding. (b) The spacer-modified master template. (c) The female mould and (d) the side view of the female mould.

moulds using an O_2 plasma cleaner (Harrick Plasma, USA) for 10 s, the polymer solutions were poured into the PDMS moulds and set at 37 °C for 10 h. After adhering a sponge tape to the base of the MN patches, they were gently and vertically peeled off from the mould and stored in a desiccator until use. In this study, two different types of MN patches (FITC MNs and FITC@CuS MNs) with PVA/PVP ratio of 5 : 10 were prepared in PBS solution. In detail, FITC MNs stand for MNs containing 20 mM FITC and FITC@CuS MNs containing 20 mM FITC and 1.2 mM CuS NPs.

The morphology and dimensions of the MN patches were imaged by a ZEISS SUPRA 55 scanning electron microscope (SEM; Carl Zeiss, Oberkochen, Germany) and an optical microscope (Nikon, Tokyo, Japan). The Universal Testing Machine (AI-7000S, Gotech, Taiwan) was used to study the MN compressive strength. Generally, a MN patch was placed on a flat rigid surface of a base plate. Then, the top workbench moved uniformly down to the MN patch at 10 μm s^{-1}. The force was recorded every second to obtain the stress–true strain relationship. The failure force was recorded when the MNs began to buckle. In addition, the microneedle patches before and after mechanical strength tests were imaged by using a digital camera with the help of a 45× hand-held loupe (YIMOO, Shenzhen, China); as a result, we ensured all the microneedles were compressed during the mechanic strength tests.

To evaluate the reproducibility of the fabrication process, we first tested the variation of the MNs length prepared using 10 moulds, which were fabricated from 10 master templates with 10 spacers in parallel. All measurements were made by using the ZEISS SUPRA 55 SEM. Using the same SEM, we further tested the uniformity of the tip size of the MNs (42 needles per array) that were prepared with the same mould in 7 sequential batches.

2.5 *In vitro* skin insertion ability of the microneedles

PVA/PVP MNs with PVA and PVP ratios of 3 : 10, 5 : 10, and 6 : 10 were applied to test the skin penetration ability. The abdominal skins of the healthy Kunming strain mice (20–25 g, the Laboratory Animal Center of Southern Medical University) were dissected and washed with 75% (v/v) ethanol solution twice prior to rinsing with 0.9% (w/v) NaCl solution once. After the skin surfaces were dried in the air, they were fixed on glass slides before the experiment. Next, the PVA/PVP MN patches were inserted into the skins gently and vertically, and a 200 g weight was placed on the center of the MNs for 5 min to ensure all the MNs were inserted into the skin tissue. Afterwards the patch was held manually for another 10 min for polymer dissolution before the MN patches were removed. These skins were imaged by an optical microscope to record the morphology of the inserted holes.

2.6 *In vitro* transdermal delivery of drugs

To study the skin penetration of drugs in the MN patches, the FITC MNs (with 6 nmol FITC per MN) were prepared with three different polymer proportions (PVA : PVP = 3 : 10, 5 : 10, and 6 : 10), which contained 500 mg mL^{-1} PVP in all solutions. The PVA/PVP MN patches were inserted into the mouse skin (abdominal skins prepared as described above) gently and vertically, and a 200 g weight was placed on the MN patches for 5 min. Afterwards, the MNs were maintained manually in place for 10 min for MN polymer dissolution in skin interstitial fluid before the MN patch was removed. The MN images before and after skin insertion were recorded by a hand-held loupe.

The *in vitro* drug permeation of the model compound FITC from MNs was investigated using a vertical Franz diffusion cell system (TP-6, Tianguang Photoelectric Instrument Co., Tianjin, China). The MN-pierced mouse skin was mounted onto the Franz cell with dermal side facing the receptor chamber. The permeation area of Franz cell was about 1.77 cm^2 (diameter: 1.5 cm). The receptor chamber was filled with 20 mL of PBS solution (pH 7.4), and the Franz diffusion cell was placed in a water bath at 37 °C and stirred at 600 rpm in the dark. At each time point, *i.e.*, 4, 8, 12, 24, 28, 36, 48, 58, and 70 h, 200 μL of the sample solution in the receptor chamber was collected and replaced with the equal volume of fresh PBS solution. Subsequently, the samples collected from the chambers were stored at −20 °C until analysis by fluorescence spectrometry using a plate reader (SpectraMax M5e, Molecular Devices, San Jose, CA, USA) with excitation and emission at 494 and 520 nm, respectively, of which the fluorescence intensity was correlated to FITC concentration using a standard curve.

In addition, the FITC@CuS MNs (with 6 nmol FITC and 0.36 nmol CuS per MN) were also applied to study the photo-activated transdermal drug permeation. The experimental process was similar to that was described above. Specially, at time points 4, 8, 12, 18, and 23 h, before near-infrared (NIR) irradiation with a laser, 200 μL solution in the receptor chamber was collected and replaced with the equal volume of fresh PBS solution. Afterwards, the skin was irradiated with an 850 nm NIR laser (1000 mW) to reach 50 °C for 5 min. After the irradiation at each time point, 200 μL solution was collected again and replaced with the equal volume of fresh PBS solution. The samples without NIR irradiation were used as controls. All the measurements were performed in triplicate.

3. Results and discussion

In this study, we developed a simple and cost-effective method (Fig. 1a) for MN patch fabrication by modifying commercial stainless-steel MN arrays as the master template, which cost approximately 1 USD and are commonly used as a tattoo needle cartridge. There are various needle cartridges with different needle dimensions and densities available in the cosmetics market, which can be easily modified as MN patch master templates.[38] Because the master template needle length must be <1 mm to form a female MN mould, the commercial tattoo needle cartridge was modified to meet the needle length requirement by forming a polymeric spacer on its bottom. The spacer was prepared from polydimethylsiloxane (PDMS) following a pouring procedure including three steps, *i.e.*, building a reaction chamber around the needle cartridge using an adhesive tape; pouring 100 μL of PDMS pre-polymer mixture

consisting of non-cross-linked PDMS liquid and crosslinking agent followed by a heat-curing treatment at 80 °C, and 20 μL of non-stick layer of 1% (w/v) PVA was added as a releasing agent. The spacer height, and thus the MN length, were adjusted by varying the PDMS volume. The tattoo cartridge and spacer assembly were thereafter used as a MN patch master template (Fig. 1b).

Fabrication of female moulds was easily accomplished in microplates by filling the wells with PDMS pre-polymer solution, introducing the master template, heat-curing the PDMS, and peeling off the master templates, which was facilitated by the previously applied PVA releasing agent layer. A fabricated female MN mould is presented in Fig. 1c and d where the length, base diameter, and needle tip microvoid diameter are 800 ± 13, 350 ± 7, and 20 ± 3 μm, respectively. The formed female mould, a precise replica of the master template, delivered the needle sizes to the final polymeric MNs. Finally, polymeric MN patches were prepared using a combination of two US FDA approved pharmaceutic and food excipient polymers, PVP[39,40] and PVA.[41] After a brief oxygen plasma treatment to increase the hydrophilicity of the microvoid surface,[42] the polymers were introduced to the mould (Fig. S1†). The polymer combination exploits the advantages of both polymers and overcomes the disadvantages of using each individually, increasing the MN mechanical strength and reducing the fabrication time and temperature, which extends their applicability to heat sensitive drugs. The polymers were mixed in various ratios, *i.e.*, PVA : PVP = 3 : 10, 5 : 10, and 6 : 10 with encapsulated model drugs, and were poured into the microvoids of the female moulds to generate MN patches. As shown in Fig. S2,† compared with 25 °C for 10 h and 40 °C for 6 h, the optimal polymerization conditions were 40 °C for 10 h to form MNs with sufficient mechanic strength to penetrate the skin, which was suitable for a variety of bioactive compounds that could be widely used in transdermal drug development.

Compared to the current state of the art,[24,43,44] the MN patches fabricated with this method exhibit several distinctive advantages. First, the heights of MNs ($n = 5$) were 1012 ± 13 μm, 768 ± 7 μm and 510 ± 5 μm when applying 50 μL, 100 μL and 150 μL of PDMS pre-polymer solution for spacer fabrication, respectively, (Fig. 2a–d), showing great linear correlation ($R^2 = 0.996$, $n = 5$ in Fig. S3†). The data suggested that the MN length can be controlled by adjusting the volume of PDMS spacer. Therefore, MNs can be fabricated with different lengths for delivery of drugs to predetermined depth. Second, the MN patches were uniformly distributed with high precision and reproducibility. As shown in Fig. 3a, the polymeric MNs were highly uniform in terms of their morphology and geometry, evidenced by the narrow distribution of the length of each needle in one patch and among different patches. The MN lengths were 770 ± 10 μm when using 10 different moulds with a 100 μL PDMS spacer, demonstrating the high reproducibility (CV = 1.59%) of the MN patch fabrication with different moulds (Fig. 3b). Meanwhile, the mould showed excellent reusability. The diameters of the MN tips maintained constant among 7 MN patches prepared using the same mould (Fig. 3c), which demonstrated the sharpness and high uniformity of the MN patch fabrication using the same mould repeatedly. The excellent uniformity of the MN patches using either the same or different moulds is indicative of the scalability of the fabrication process. In addition, the low-cost of the master templates, high reusability of the moulds, and the suitability of the processes for automation further increase the scalability potential of the MN fabrication.

Third, controlled drug release and permeation can be achieved by changing the polymer composition. First, during the first 15 min, all of the MNs were dissociated from the base and entered the skin tissue (Fig. S4†). As shown in Fig. 4a, the permeation profiles of a model drug, *i.e.*, FITC dye, released from the polymeric MN patches showed that PVA/PVP MNs with a ratio of 3 : 10 delivered approximately 80% FITC across the skin after 48 h (the standard curve was given in Fig. S5,† $y = 0.866x - 12.939$, $R^2 = 0.9993$). In contrast, the FTIC released from patches with PVA/PVP ratios of 5 : 10 and 6 : 10 was only 55% and 35% over the same time, respectively. The results show that increased PVA proportion slows the drug release kinetics

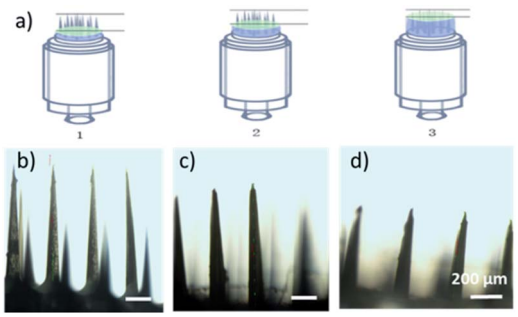

Fig. 2 (a) Length adjustment scheme. (b–d) Microneedle (MN) micrographs when using 50, 100, and 150 μL of spacer.

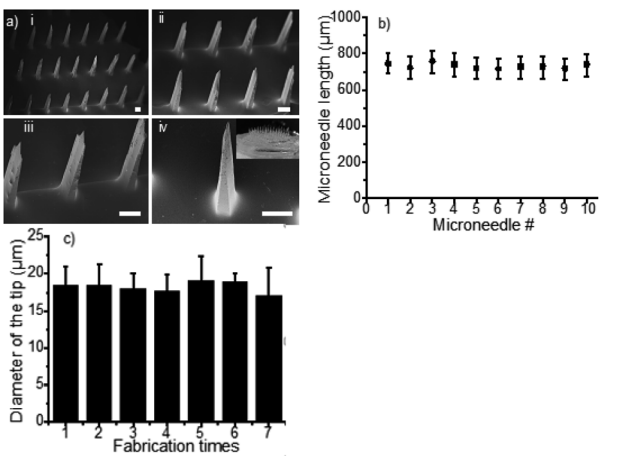

Fig. 3 (a) Scanning electron microscopy images of MNs (inset: digital camera image of a microneedle patch). (b) The length of the MNs for the 10 MN patches when using different moulds. All of the microneedle moulds were fabricated with 100 μL spacers. Error bars represent the standard deviation (SD) for $n = 10$. (c) The size of the MN tips that were prepared in 7 batches using the same mould. Error bars represent the standard deviation (SD).

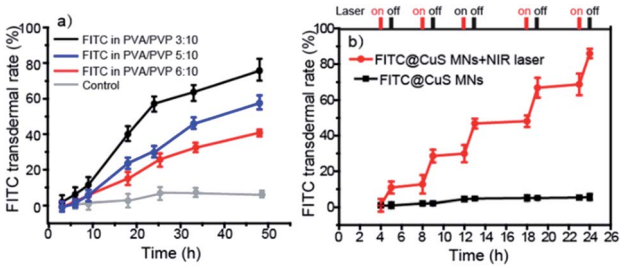

Fig. 4 Drug release profiles of the prepared microneedle (MN) patches. (a) The release profiles of the model drug FITC from the FITC-loaded MNs with varied polymer composition through mouse ventral skin. (b) NIR light-activated release behaviour of FITC@CuS MNs. The FITC release profiles of MNs that were and were not subjected to NIR light intervals. The process was controlled for 5 min at 50 °C in the laser-on state. The NIR laser had a wavelength of 850 nm. Error bars represent the standard deviation (SD) for $n = 3$.

and thus suits sustained drug release, presumably because of much slower dissolution kinetics of PVA and higher affinity of the model drug with PVA than PVP.[45] In addition, the drug release and permeation profiles could also be regulated by incorporating photothermal nanomaterials, such as CuS NPs (9 ± 4 nm, characterization in Fig. S6†) into the MNs, which triggered rapid controllable release upon irradiation by NIR light that induced dissolution of the MNs and increased diffusion of the drug molecules within the skin tissue (Fig. 4b). In contrast, the laser-off state (control) allowed for only negligible drug release over the time interval. The FITC release could be repeatedly activated by NIR light, demonstrating that the drug release from MNs containing CuS NPs and the permeation within skin tissue could be precisely regulated by the on/off state of NIR light. In this study, CuS NPs were chosen for transdermal PTT because of their biodegradability,[46,47] oxidative cytotoxicity,[48] low cost, and excellent photothermal efficiency.[49,50] We did not use gold nanomaterials, such as gold nanorods or nanocages, because they are chemically inert, costly, and not biodegradable.[51]

Last, by optimizing the polymer composition in the formula, the MN mechanical strength can be dramatically improved to pierce into the skin (Fig. S7†). The failure force curves shown in Fig. S8† show that the MNs are strong enough for transdermal drug delivery when the highest failure force of the MN material is higher than 0.03 N per needle.[52] In brief, all of these attributes, including the uniformity, scalability for high-precision production, controllable release, tenability, and mechanic strength make MN patches a promising tool for transdermal drug delivery. The limitation of the MN patch mould is that its configuration is pre-determined and limited by that of the tattoo cartridges, and is thus not modifiable; nevertheless, for most experimental research, our work provides a time- and cost-effective way to fabricate MN patches.

4. Conclusions

We have reported a simple and cost-effective method to fabricate the polymeric MN templates by modifying commercial stainless-steel MN arrays with a PDMS spacer. Importantly, the templates are tunable and versatile. Using the templates, dissolvable polymeric MNs were fabricated with high precision and uniformity. Though the structure and aspect ratios of the MNs are pre-determined by the commercial stainless-steel MN arrays, and are thus not easily modifiable, the composition of the polymer formulation and the length of the MNs are tunable, providing sufficient room for optimization of the MNs to realize specific therapeutic aims, which is especially useful for pre-clinical proof-of-concept studies. Therefore, our findings may accelerate both academic research and industrial production of polymeric MNs patches for transdermal drug delivery.

Conflicts of interest

There are no conflicts to declare.

Acknowledgements

This work was supported by Beatrice Hunter Cancer Research Institute (BHCRI), China Postdoctoral Science Foundation (2019M653139), Guangdong Province Higher Vocational College & School's Pearl River Scholar Funded Scheme (2017), Canada Research Chairs program, New Frontiers in Research Fund - Exploration (NFRFE-2018-01005), the Scientific and Technological Foundation of Shenzhen, China (GJHZ20180928161212140), Cape Breton University RISE program, NSERC Discovery Grants Program, and Post-doctoral Foundation Project of Shenzhen Polytechnic (6019330001K, 6019330006K, and 6019330007K).

References

1 S. Henry, D. V. McAllister, M. G. Allen and M. R. Prausnitz, *J. Pharm. Sci.*, 1998, **87**, 922–925.
2 M. R. Prausnitz and R. Langer, *Nat. Biotechnol.*, 2008, **26**, 1261–1268.
3 M. R. Prausnitz, *Annu. Rev. Chem. Biomol. Eng.*, 2017, **8**, 177–200.
4 Y. Ye, J. Yu, D. Wen, A. R. Kahkoska and Z. Gu, *Adv. Drug Deliv. Rev.*, 2018, **127**, 106–118.
5 W. Sun, M. Inayathullah, M. A. C. Manoukian, A. V. Malkovskiy, S. Manickam, M. P. Marinkovich, A. T. Lane, L. Tayebi, A. M. Seifalian and J. Rajadas, *Ann. Biomed. Eng.*, 2015, **43**, 2978–2990.
6 A. A. Ali, C. M. McCrudden, J. McCaffrey, J. W. McBride, G. Cole, N. J. Dunne, T. Robson, A. Kissenpfennig, R. F. Donnelly and H. O. McCarthy, *J. Nanomed. Nanotechnol.*, 2017, **13**, 921–932.
7 G. Yao, G. Quan, S. Lin, T. Peng, Q. Wang, H. Ran, H. Chen, Q. Zhang, L. Wang, X. Pan and C. Wu, *Int. J. Pharm.*, 2017, **534**, 378–386.
8 A. M. S, M. Soltani, P. Najafizadeh, S. A. Ebrahimi and P. Chen, *J. Controlled Release*, 2017, **261**, 87–92.
9 S. Lin, G. Quan, A. Hou, P. Yang, T. Peng, Y. Gu, W. Qin, R. Liu, X. Ma, X. Pan, H. Liu, L. Wang and C. Wu, *J. Controlled Release*, 2019, **306**, 69–82.

10 J. Mao, H. Wang, Y. Xie, Y. Fu, Y. Li, P. Liu, H. Du, J. Zhu, L. Dong, M. Hussain, Y. Li, L. Zhang, J. Zhu and J. Tao, *J. Mater. Chem. B*, 2020, **8**, 928–934.
11 J. Kennedy, E. Larraneta, M. T. C. McCrudden, C. M. McCrudden, A. J. Brady, S. J. Fallows, H. O. McCarthy, A. Kissenpfennig and R. F. Donnelly, *J. Controlled Release*, 2017, **265**, 57–65.
12 W. Chen, R. Tian, C. Xu, B. C. Yung, G. Wang, Y. Liu, Q. Ni, F. Zhang, Z. Zhou, J. Wang, G. Niu, Y. Ma, L. Fu and X. Chen, *Nat. Commun.*, 2017, **8**, 1777.
13 C. Wang, Y. Ye, G. M. Hochu, H. Sadeghifar and Z. Gu, *Nano Lett.*, 2016, **16**, 2334–2340.
14 X. He, J. Sun, J. Zhuang, H. Xu, Y. Liu and D. Wu, *Dose-Response*, 2019, **17**, 1559325819878585.
15 G. Ma and C. Wu, *J. Controlled Release*, 2017, **251**, 11–23.
16 S. Bhatnagar, K. Dave and V. V. K. Venuganti, *J. Controlled Release*, 2017, **260**, 164–182.
17 S. Duarah, M. Sharma and J. Wen, *Eur. J. Pharm. Biopharm.*, 2019, **136**, 48–69.
18 M. Wang, L. Hu and C. Xu, *Lab Chip*, 2017, **17**, 1373–1387.
19 M. J. Mistilis, J. C. Joyce, E. S. Esser, I. Skountzou, R. W. Compans, A. S. Bommarius and M. R. Prausnitz, *Drug Delivery Transl. Res.*, 2017, **7**, 195–205.
20 D. V. McAllister, P. M. Wang, S. P. Davis, J.-H. Park, P. J. Canatella, M. G. Allen and M. R. Prausnitz, *Proc. Natl. Acad. Sci. U. S. A.*, 2003, **100**, 13755–13760.
21 N. W. Kim, S. Y. Kim, J. E. Lee, Y. Yin, J. H. Lee, S. Y. Lim, E. S. Kim, H. T. T. Duong, H. K. Kim, S. Kim, J. E. Kim, D. S. Lee, J. Kim, M. S. Lee, Y. T. Lim and J. H. Jeong, *ACS Nano*, 2018, **12**, 9702–9713.
22 P. Singh, A. Carrier, Y. Chen, S. Lin, J. Wang, S. Cui and X. Zhang, *J. Controlled Release*, 2019, **315**, 97–113.
23 Y. Chen, Y. Yang, Y. Xian, P. Singh, J. Feng, S. Cui, A. Carrier, K. Oakes, T. Luan and X. Zhang, *ACS Appl. Mater. Interfaces*, 2019, **12**, 352–360.
24 T. N. Tarbox, A. B. Watts, Z. Cui and R. O. Williams 3rd, *Drug Delivery Transl. Res.*, 2018, **8**, 1828–1843.
25 Q. L. Wang, D. D. Zhu, Y. Chen and X. D. Guo, *Mater. Sci. Eng., C*, 2016, **65**, 135–142.
26 J. D. Kim, M. Kim, H. Yang, K. Lee and H. Jung, *J. Controlled Release*, 2013, **170**, 430–436.
27 P. Dardano, A. Calio, V. Di Palma, M. F. Bevilacqua, A. Di Matteo and L. De Stefano, *Materials*, 2015, **8**, 8661–8673.
28 T. Tomono, *Microsyst. Technol.*, 2018, **24**, 3589–3599.
29 C. P. P. Pere, S. N. Economidou, G. Lall, C. Ziraud, J. S. Boateng, B. D. Alexander, D. A. Lamprou and D. Douroumis, *Int. J. Pharm.*, 2018, **544**, 425–432.
30 M. A. Luzuriag, D. R. Berry, J. C. Reagan, R. A. Smaldone and J. J. Gassensmith, *Lab Chip*, 2018, **18**, 1223–1230.
31 Z. Chen, L. Ren, J. Li, L. Yao, Y. Chen, B. Liu and L. Jiang, *Acta Biomater.*, 2018, **65**, 283–291.
32 R. Vecchione, S. Coppola, E. Esposito, C. Casale, V. Vespini, S. Grilli, P. Ferraro and P. A. Netti, *Adv. Funct. Mater.*, 2014, **24**, 3515–3523.
33 J. A. Rogers, Z. Bao, K. Baldwin, A. Dodabalapur, B. Crone, V. R. Raju, V. Kuck, H. Katz, K. Amundson, J. Ewing and P. Drzaic, *Proc. Natl. Acad. Sci. U. S. A.*, 2001, **98**, 4835–4840.
34 S. Chen, D. Wu, Y. Liu, Y. Huang, H. Xu, W. Gao, J. Zhang, J. Sun and J. Zhuang, *J. Drug Delivery Sci. Technol.*, 2020, **56**, 101547.
35 J. Zhuang, D. M. Wu, H. Xu, Y. Huang, Y. Liu and J. Y. Sun, *Int. Polym. Process.*, 2019, **34**, 231–238.
36 M. Zhou, R. Zhang, M. Huang, W. Lu, S. Song, M. P. Melancon, M. Tian, D. Liang and C. Li, *J. Am. Chem. Soc.*, 2010, **132**, 15351–15358.
37 W. Gao, Y. Sun, M. Cai, Y. Zhao, W. Cao, Z. Liu, G. Cui and B. Tang, *Nat. Commun.*, 2018, **9**, 231.
38 M. T. McCrudden, E. McAlister, A. J. Courtenay, P. Gonzalez-Vazquez, T. R. Singh and R. F. Donnelly, *Exp. Dermatol.*, 2015, **24**, 561–566.
39 S. P. Sullivan, N. Murthy and M. R. Prausnitz, *Adv. Mater.*, 2008, **20**, 933–938.
40 W. Sun, Z. Araci, M. Inayathullah, S. Manickam, X. Zhang, M. A. Bruce, M. P. Marinkovich, A. T. Lane, C. Milla, J. Rajadas and M. J. Butte, *Acta Biomater.*, 2013, **9**, 7767–7774.
41 H. X. Nguyen, B. D. Bozorg, Y. Kim, A. Wieber, G. Birk, D. Lubda and A. K. Banga, *Eur. J. Pharm. Biopharm.*, 2018, **129**, 88–103.
42 I. C. Lee, J.-S. He, M.-T. Tsai and K.-C. Lin, *J. Mater. Chem. B*, 2015, **3**, 276–285.
43 S. Gholami, M. M. Mohebi, E. Hajizadeh-Saffar, M. H. Ghanian, I. Zarkesh and H. Baharvand, *Int. J. Pharm.*, 2019, **558**, 299–310.
44 R. E. M. Lutton, E. Larrañeta, M.-C. Kearney, P. Boyd, A. D. Woolfson and R. F. Donnelly, *Int. J. Pharm.*, 2015, **494**, 417–429.
45 R. Oun, J. A. Plumb and N. J. Wheate, *J. Inorg. Biochem.*, 2014, **134**, 100–105.
46 Z. Xiao, *Nanomedicine*, 2014, **9**, 373–375.
47 L. Dong, K. Li, D. Wen, Y. Lu, K. Du, M. Zhang, X. Gao, J. Feng and H. Zhang, *Nanoscale*, 2019, **11**, 12853–12857.
48 L. Wang, Y. Miao, M. Lu, Z. Shan, S. Lu, J. Hou, Q. Yang, X. Liang, T. Zhou, D. Curry, K. Oakes and X. Zhang, *Chem. Commun.*, 2017, **53**, 5862–5865.
49 K. Dong, Z. Liu, Z. Li, J. Ren and X. Qu, *Adv. Mater.*, 2013, **25**, 4452–4458.
50 N. Li, Q. Sun, Z. Yu, X. Gao, W. Pan, X. Wan and B. Tang, *ACS Nano*, 2018, **12**, 5197–5206.
51 Y. P. Jia, B. Y. Ma, X. W. Wei and Z. Y. Qian, *Chin. Chem. Lett.*, 2017, **28**, 691–702.
52 R. F. Donnelly, T. R. Singh, M. J. Garland, K. Migalska, R. Majithiya, C. M. McCrudden, P. L. Kole, T. M. Mahmood, H. O. McCarthy and A. D. Woolfson, *Adv. Funct. Mater.*, 2012, **22**, 4879–4890.

